Ground state magnetic dipole moment of ^{40}Sc

Robert Powel,[1,2] B. Alex Brown,[1,2] J. D. Holt,[3] Andrew Klose,[4] Kristian König,[1] Jeremy Lantis,[1,5] Kei Minamisono,[1,2,*] T. Miyagi,[3,6,7] and Skyy Pineda[1,5]

[1]*National Superconducting Cyclotron Laboratory, Michigan State University, East Lansing, Michigan 48824, USA*
[2]*Department of Physics and Astronomy, Michigan State University, East Lansing, Michigan 48824, USA*
[3]*TRIUMF, Vancouver, British Columbia, V6T 2A3 Canada*
[4]*Department of Chemistry and Biochemistry, Augustana University, Sioux Falls, South Dakota 57197, USA*
[5]*Department of Chemistry, Michigan State University, East Lansing, Michigan 48824, USA*
[6]*Technische Universität Darmstadt, Department of Physics, 64289 Darmstadt, Germany*
[7]*ExtreMe Matter Institute EMMI, GSI Helmholtzzentrum für Schwerionenforschung GmbH, 64291 Darmstadt, Germany*

(Received 18 January 2022; accepted 18 February 2022; published 9 March 2022)

The hyperfine coupling constants of the proton dripline odd-odd ^{40}Sc nucleus were deduced from the hyperfine spectrum of the $3d4s\,^3\mathrm{D}_2 \leftrightarrow 3d4p\,^3\mathrm{F}^\circ_3$ transition in Sc II, measured by the bunched beam collinear laser spectroscopy technique. The ground-state magnetic-dipole and electric-quadrupole moments were determined as $\mu = +5.57(4)(2)\mu_N$ and $Q = +42(38)(28)\ e^2\,\mathrm{fm}^2$, respectively. The magnetic moment is well reproduced by the additivity rule with magnetic moments of neighboring odd-even nuclei in the vicinity of the doubly magic ^{40}Ca nucleus. An *ab initio* multishell valence-space Hamiltonian was also employed to calculate the magnetic moment of ^{40}Sc, which spans across the *sd* and *fp* nuclear shells, where we obtained good agreements.

DOI: 10.1103/PhysRevC.105.034310

I. INTRODUCTION

Ground-state magnetic-dipole moments of radioactive nuclei have played a crucial role in understanding their structure. A magnetic moment is a one body operator acting on a single nuclear state, is complementary to magnetic transition moments, and is sensitive to how valence nucleons are arranged inside a nucleus, namely, the nuclear wave function. Each of the single-particle proton and neutron state in the nuclear shell model has a distinct magnetic moment, the so-called Schmidt [1] or single-particle value. Any departure from the single-particle value indicates requirements of the configuration mixing of valence protons and neutrons, and/or mesonic effects.

In the present study the ground-state magnetic moment of the $^{40}\mathrm{Sc}(I = 4^-,\ T_{1/2} = 182.3$ ms) nucleus was determined by using the bunched beam collinear laser spectroscopy technique. The ^{40}Sc nucleus occurs in the vicinity of the stable doubly magic ^{40}Ca with one more proton and one less neutron to the ^{40}Ca nucleus. The ^{40}Sc nucleus, however, is situated at the proton drip line, since ^{39}Sc at one less neutron is known to be unbound against the one proton emission [2]. Furthermore, due to the nature of the odd-odd nucleus with nucleon configuration across the *sd* (one neutron hole in $d_{3/2}$ shell) and *fp* (one proton in the $f_{7/2}$ shell) major shells and possible valence proton-neutron interactions, it is notoriously challenging to reproduce the experimental magnetic moments by any theoretical calculations.

In the single-particle (sp) model, the magnetic moment of an odd-even, half-integer isospin nucleus is given by the projection theorem and determined by the last unpaired nucleon in the odd nuclei group [1] as

$$\mu_{\rm sp} = I\left(g^l \pm \frac{g^s - g^l}{2l+1}\right), \tag{1}$$

where superscripts l and s are for the orbital and spin angular momentum, respectively, and nuclear spin I is given by $I = l \pm 1/2$. The free nucleon g factors are given by $g^l_p = 1$, $g^s_p = 5.5855$, $g^l_n = 0$ and $g^s_n = -3.826$. It is well known that magnetic moments appear in between these single-particle lines [3] for $I = l \pm 1/2$ with one exception of ^{9}C due to the charge symmetry breaking [4–6]. Magnetic moments of magic nuclei appear closer to these single-particle lines, and open-shell nuclei being away from the lines, indicating a departure from the single-particle model and increasing contribution from the nucleon configuration mixing.

On the other hand, the magnetic moment of an odd-odd, integer isospin nucleus is determined in the single-particle model by the last unpaired proton and neutron, and can be obtained by a sum of corresponding single-particle moments of neighboring odd-even nuclei [7,8]:

$$\begin{aligned} \vec{I} &= \vec{I}_p + \vec{I}_n, \\ \mu_I &= \langle IM|g_p\vec{I}_p + g_n\vec{I}_n|IM\rangle_{M=I}. \end{aligned} \tag{2}$$

Here, I and μ_I are the spin and magnetic moment of the odd-odd nucleus, respectively, and I_p (g_p) and I_n (g_n) are the spin (g factor) of the neighboring nucleus with unpaired proton and neutron, respectively. The magnetic moment can

*minamiso@nscl.msu.edu

then be obtained as

$$\mu_I = \frac{I}{2I_p}\left\{1 + \frac{(I_p - I_n)(I_p + I_n + 1)}{I(I+1)}\right\}\mu_p + \frac{I}{2I_n}\left\{1 + \frac{(I_n - I_p)(I_p + I_n + 1)}{I(I+1)}\right\}\mu_n, \quad (3)$$

where $\mu_x = g_x I_x$ with the subscript x for p or n. We call this relation the additivity rule hereafter in this paper. Many magnetic moments of such odd-odd nuclei are known near stable isotopes [9] and compared with single-particle values based on the additivity rule [10]. For ^{40}Sc, μ_p and μ_n correspond to magnetic moments of ^{41}Sc and ^{39}Ca, respectively. It is of primary interest of the present study whether the magnetic moment of proton drip-line ^{40}Sc can be expressed using know magnetic moments of its neighboring semimagic nuclei, ^{41}Sc and ^{39}Ca, which occur near the doubly magic ^{40}Ca according to the additivity rule. ^{41}Sc and ^{39}Ca are doubly magic plus or minus one nucleon nuclei and their magnetic moments are supposed to be close to the single-particle values. However, it has been shown that sizable cross shell excitations are required to reproduce their magnetic moments [11,12]. In addition to shell-model calculations, recently developed valence-space in-medium similarity renormalization-group calculations for multiple major-oscillator shells were also applied for the magnetic moment of ^{40}Sc to benchmark such calculations for an odd-odd nucleus requiring cross shell excitations.

II. HYPERFINE INTERACTION

The shift of an atomic energy level due to the hyperfine (hf) interaction relative to an atomic fine-structure level is given by

$$\begin{aligned} \frac{\Delta E}{h} &= \alpha A^{\mathrm{hf}} + \beta B^{\mathrm{hf}}, \\ \alpha &= \frac{K}{2}, \\ \beta &= \frac{3K(K+1) - 4I(I+1)J(J+1)}{8I(2I-1)J(2J-1)}, \\ K &= F(F+1) - I(I+1) - J(J+1). \end{aligned} \quad (4)$$

Here I and J are the total angular momenta or spins of the nucleus and electrons, respectively, and F is the quantum number associated with the total angular momentum of the atom defined by $\mathbf{F} = \mathbf{I} + \mathbf{J}$. The A^{hf} and B^{hf} are the hyperfine coupling constants defined as

$$A^{\mathrm{hf}} = \frac{\mu B(0)}{IJ}, \quad (5)$$

$$B^{\mathrm{hf}} = eQ\left\langle \frac{\partial^2 V_e}{\partial z^2} \right\rangle, \quad (6)$$

where $B(0)$ is the magnetic field generated by the atomic electrons at the center of the nucleus, e is the electric unit charge, Q is the spectroscopic nuclear electric-quadrupole moment, and $\langle \partial^2 V_e/\partial z^2 \rangle$ is the electric-field gradient produced by the atomic electrons at the center of the nucleus. The magnetic field and the electric-field gradient are isotope independent, assuming a point-like nucleus (the hyperfine anomalies [13] are neglected here). According to Eqs. (5) and (6), unknown nuclear moments may be deduced from the measured hyperfine coupling constants using a reference nucleus of the same element, whose hyperfine coupling constants for the same electronic level and nuclear moments are known. A simple ratio of hyperfine coupling constants derives nuclear moments as

$$\mu = \mu_{\mathrm{R}} \frac{A^{\mathrm{hf}}}{A^{\mathrm{hf}}_{\mathrm{R}}} \frac{I}{I_{\mathrm{R}}}, \quad (7)$$

$$Q = Q_{\mathrm{R}} \frac{B^{\mathrm{hf}}}{B^{\mathrm{hf}}_{\mathrm{R}}}, \quad (8)$$

where the subscript R indicates a reference nucleus. If a suitable reference isotope does not exist, the magnetic field and electric-field gradient may be obtained by theoretical calculations. In the present study ^{45}Sc was used as the reference isotope.

The transition frequency ν of an electronic transition between a pair of hyperfine levels can be expressed using five parameters as

$$\nu = \nu_0 + \left(\alpha_u A^{\mathrm{hf}}_u + \beta_u B^{\mathrm{hf}}_u\right) - \left(\alpha_l A^{\mathrm{hf}}_l + \beta_l B^{\mathrm{hf}}_l\right), \quad (9)$$

where ν_0 is the center-of-gravity (COG) frequency, and the u and l subscripts refer to the upper and lower hyperfine states of the transition, respectively. The α and β are constants determined by the nuclear and atomic spins of the specific transition given by Eq. (4).

III. EXPERIMENT

The radioactive ^{40}Sc ion beam was produced by the one-proton pickup and one-neutron removal reaction of a primary ^{40}Ca beam on a natural Be target. The ^{40}Ca beam was accelerated to 140 MeV/A in the coupled cyclotrons at the National Superconducting Cyclotron Laboratory at Michigan State University. The produced fast ^{40}Sc ion beam was separated in the A1900 fragment separator [14] from other reaction products, thermalized in a gas cell [15] filled with a helium buffer gas, and extracted by rf and DC electric fields as singly charged ions at an energy of 30 keV.

The low-energy ^{40}Sc ion beam was then transported to the beam cooler and laser spectroscopy (BECOLA) facility [16,17], where the ion beam was injected into a radio frequency quadrupole (RFQ) cooler-buncher [18] filled with a helium-buffer gas. Buffer gas pressures in the RFQ were ≈100 mTorr and ≈1 mTorr in the cooling and bunching sections, respectively. The ions were collected for 300 ms and then released in bunches with a typical temporal width of 1 μs (full width at half maximum) at an approximate energy of 29 850 eV and transported to the collinear laser spectroscopy (CLS) beam line. By selecting photons only within the time window of beam bunches [17], the photon background originating from scattered laser light can be dramatically reduced [19,20]. In the present measurement a background suppression factor was 3×10^5.

The ions were then collinearly overlapped with laser light for laser-resonant fluorescence measurement. Fluorescence was detected by a photon detection unit consisting of a mirror based light collector [21], which eliminates background and focuses resonant fluorescence onto a photomultiplier tube. A scanning voltage was applied to the photon detection unit, which is electronically isolated from the ground potential to vary the ion-beam velocity and to scan the Doppler-shifted laser frequency across the hyperfine spectrum. The voltage scanning range is typically −2 to 2 kV. The induced fluorescence was then detected by the photon detection unit as a function of the applied scanning voltage.

Typical rates of ^{40}Sc and ^{41}Sc at the entrance to the RFQ were 15×10^3 and 20×10^3 ions/s, respectively. There was a large contamination of ^{40}Ar ions ($>10^7$ s^{-1}) in the ^{40}Sc beam, due to the trace amount argon component in the helium buffer gas of the gas stopping cell. The RFQ can accept typically 10^6 ions for trapping and bunching. When more ions are injected, some of ions are lost and measured hyperfine spectra become distorted due to the excess space charge in the trap [18]. To avoid this overfilling, ^{40}Sc hyperfine spectra were measured with faster bunching cycle (20 ms) at the cost of the background suppression. The total data accumulation time for ^{40}Sc and ^{41}Sc were 70 and 30 hours, respectively. The longer accumulation time for ^{40}Sc is mainly due to the ^{40}Ar contamination.

The hyperfine spectrum of $3d4s\,^3\mathrm{D}_2 \leftrightarrow 3d4p\,^3\mathrm{F}^{\circ}_3$ transition in Sc II at 363 nm was measured. Laser light at 726 nm was produced by a Sirah Matisse TS Ti:sapphire ring laser, which was then frequency doubled to 363 nm using a SpectraPhysics Wavetrain. The laser frequency of the Ti:sapphire laser was measured and stabilized by a HighFinesse WSU-30 wavelength meter, calibrated every minute by a frequency-stabilized helium-neon laser. The 363 nm laser light was collimated to a beam diameter of approximately 1 mm. The laser light was aligned to go through the center of the photon-detection region using two 2.5-m-separated 3 mm apertures in the BECOLA beamline. Three photon detection units were placed in series along the ion-beam direction to detect the resonant fluorescence.

Every few hours throughout the data accumulation, the radioactive Sc beam was stopped and a stable ^{45}Sc beam was introduced into the CLS beam line for about an hour for calibration purposes. The ^{45}Sc ion beam was produced using a Penning Ionization Gauge ion source [22] installed upstream of the RFQ. Fluorescence spectra of ^{45}Sc were measured as a reference to determine the resonance lineshape and to monitor the time-dependent centroid shift due mainly to the voltage shift caused by the temperature variation over a week-long running time. The number of ^{45}Sc ions in a bunch was limited to about 10^5 to keep a similar space-charge condition in the trap as to radioactive beam measurements, but the data collection was done with a higher beam-bunch repetition rate of 100 Hz to efficiently collect calibration data.

IV. EXPERIMENTAL RESULTS

A. Hyperfine spectra

The obtained hyperfine spectra for the $3d4s\,^3\mathrm{D}_2 \leftrightarrow 3d4p\,^3\mathrm{F}^{\circ}_3$ transition are shown in Fig. 1 for ^{40}Sc, ^{41}Sc, and ^{45}Sc. The solid dots are the data and the solid line is a result of a lineshape fit. ^{40}Sc, ^{41}Sc, and ^{45}Sc have nuclear spins of 4, 7/2, and 7/2, respectively, and have 15 allowed hyperfine transitions, which were not all observed for ^{40}Sc and ^{41}Sc due to the achievable signal-to-noise ratio in a limited beam time given the sensitivity of the detection system. Especially for ^{40}Sc, a large amount of ^{40}Ar contamination in the beam prevented the background suppression by the bunched-beam CLS technique, due to the overfilling of the RFQ ion trap.

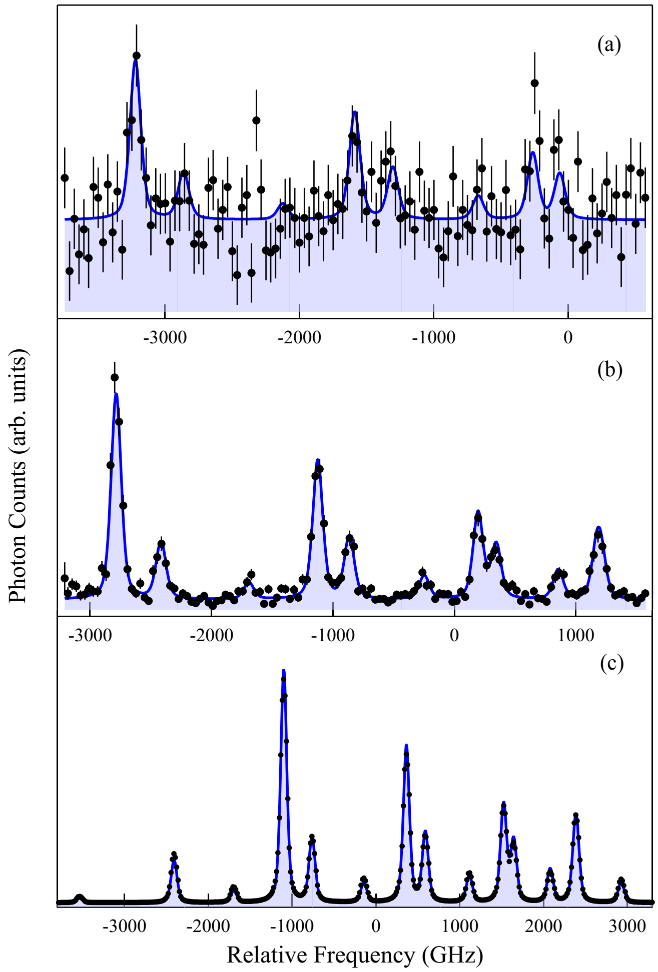

FIG. 1. Obtained hyperfine spectra of $3d4s\,^3\mathrm{D}_2 \leftrightarrow 3d4p\,^3\mathrm{F}^{\circ}_3$ transition in Sc II for (a) ^{40}Sc, (b) ^{41}Sc, and (c) ^{45}Sc. The horizontal axes are relative to the center-of-gravity resonance frequency of the ^{45}Sc hyperfine spectrum. The vertical bars are statistical uncertainties. For ^{45}Sc the statistical uncertainties are within the dots and not shown in the figure. The solid blue lines and shades are results of the fits. For ^{40}Sc and ^{41}Sc not all allowed transitions were observed due to the sensitivity of the detection unit.

The hyperfine spectra were fit using a pseudo-Voigt lineshape with all peaks having a common width and Lorentzian-Gaussian fraction. The relative peak amplitudes for all spectra were fixed to ratios among transition probabilities of hyperfine transitions determined by the quantum numbers (I, J, and F) of the lower and upper levels, and the overall amplitude was determined by the fit. The individual peak frequency can be expressed using five parameters as in Eq. (9), namely, A^{hf} and B^{hf} coefficients for lower and upper

TABLE I. Hyperfine coupling constants for the $^3D_2 \leftrightarrow ^3F_3^\circ$ electronic transition in ^{40,41,45}Sc extracted from the fit of the hyperfine spectra. For ^{40,41}Sc the $^3D_1 \leftrightarrow ^3P_0$ transition was also measured and coupling constants for the $^3D_1$ state are also summarized. The low statistics of the ^{40}Sc data gives possible uncertainties in the fitting procedure. These fitting uncertainties were estimated from the variation of several different fitting procedures and were included in the uncertainties shown for ^{40}Sc.

Isotope	A^{hf} (MHz)			B^{hf} (MHz)		
	$^3D_1$	$^3D_2$	$^3F_3^\circ$	$^3D_1$	$^3D_2$	$^3F_3^\circ$
^{40}Sc(4^-)		+520.1(39)(18)	+210.7(16)(08)[a]		+58(52)(39)	+106(95)(66)[b]
^{41}Sc($7/2^-$)	−549.4(16)(1)	+579.7(12)(01)	+234.81(76)(04)	−16(10)(0)	−25(14)(0)	−26(17)(0)
^{45}Sc($7/2^-$)	−479.58(3)(3)	+507.54(2)(4)	+205.57(17)(12)	−11.7(1)(0)	−32.63(21)(15)	−59.27(24)(5)

[a]The ratio to $A^{hf}(^3D_2)$ was fixed relative to that of ^{45}Sc.
[b]The ratio to $B^{hf}(^3D_2)$ was fixed relative to that of ^{45}Sc.

levels of the transition and the COG frequency, all of which were allowed to vary freely in the fitting procedure.

Due to the poor signal-to-noise ratio of the ^{40}Sc data, the peak width and Lorentzian-Gaussian fraction determined by the hyperfine spectrum of ^{41}Sc, which has greater signal-to-noise ratio, were used to constrain the fit of the ^{40}Sc spectrum. Furthermore, the hyperfine coupling constants were constrained to match the ratio of coupling constants of our precise measurements of stable ^{45}Sc as $A_l^{hf}/A_u^{hf} = 2.4689(5)$ and $B_l^{hf}/B_u^{hf} = 0.55(2)$. The uncertainties of the ratios were taken into account as systematic uncertainties of ^{40}Sc hyperfine coupling constants, which are small compared with the statistical uncertainties of the ^{40}Sc results. With these constraints and known nuclear spin of four, the fit result was uniquely obtained from the pattern of the observed hf spectrum, although not all allowed transitions were detected.

B. Corrections

The COG frequency of the $^3D_2 \leftrightarrow ^3F_3^\circ$ transition was determined to be 825 470 305(2)(20) MHz in a separate offline measurement using collinear and anticollinear laser spectroscopy technique on stable ^{45}Sc. The first parentheses of the COG frequency is for the statistical uncertainty and the second is for the systematic uncertainty due to the laser frequency measurement using the WSU-30 wavelength meter. The COG frequency was used to calibrate the Sc ion-beam energy in the online ^{40}Sc hyperfine spectrum measurements. The ^{45}Sc calibration spectra were used to deduce the ion-beam energy as described in Ref. [25], where the 20 MHz systematic uncertainty in the COG is mostly canceled. The ion-beam energy was determined with less than 0.3 eV uncertainty, which contributes to the systematic uncertainties of the stable hyperfine coupling constants by less than 10 ppm.

A correction for the nonlinearity of scanning voltage was applied to the hyperfine spectra due to a penetration of the static electromagnetic field applied to the detection region for the Doppler tuning. The nonlinear behavior in the scanning voltage would stretch or shrink the hyperfine spectrum observed, which would then affect the deduced hyperfine coupling constants. This correction was estimated by comparing the isotope shift between ^{40}Ca and ^{44}Ca measured at BECOLA to the well-known literature values. A correction of 550(50) ppm was estimated and applied to the present hyperfine coupling constants. The uncertainty is included in the systematic uncertainties of the hyperfine coupling constants. The voltmeter used to measure the scanning voltage was rated to have an approximate uncertainty of 80 ppm, which is also included in the systematic uncertainties. Both contributions to the total systematic uncertainty are negligibly small compared with the statistical and other systematic uncertainties of ^{40}Sc.

Determined hyperfine coupling constants are summarized in Table I. Signs are explicitly given for all experimental numbers hereafter. The statistical and systematic uncertainties are shown in the first and second parentheses, respectively. For ^{40}Sc, an additional systematic contribution is considered resulting from the correlation between A^{hf} and B^{hf} coupling constants in the fitting procedure. Especially the B^{hf} has large uncertainty that affects the determination of A^{hf}. To estimate the effect of the uncertainty of B^{hf} on A^{hf}, we varied and fixed B^{hf} in the fitting procedure, and take the variation in A^{hf} as the systematic uncertainty of A^{hf}.

C. Magnetic-dipole moment

The magnetic-dipole hyperfine coupling constant of the $3d4s\ ^3D_2$ state in ^{40}Sc was obtained as

$$A^{hf}(^3D_2) = +520.1(39)(18)\ \text{MHz}.$$

The magnetic moment of ^{40}Sc can be deduced from Eq. (7) together with the $A^{hf}(^3D_2)$ and the magnetic moment of ^{45}Sc as

$$\mu(^{40}\text{Sc}) = \mu(^{45}\text{Sc}) \frac{A^{hf}(^{40}\text{Sc})}{A^{hf}(^{45}\text{Sc})} \frac{I(^{40}\text{Sc})}{I(^{45}\text{Sc})}. \tag{10}$$

Here it is noted that deviation from a point-like nucleus, the hyperfine anomaly [13], and its effect on hyperfine coupling constants is not known for any of the atomic states in Sc isotopes [26]. The hyperfine anomaly is typically smaller than the relative uncertainty of ≈1% in the present result for magnetic moment and is therefore neglected in the present analysis. The magnetic moment of reference ^{45}Sc was evaluated from the ratio of NMR frequencies between ^{45}Sc (in a solution of $ScCl_3$ in acidified deuterium water) and deuterium $(^{45}\text{Sc})/\nu(D) = 1.582\,453\,4(6)$ [24]. Using values of the ratio between NMR frequencies of hydrogen in H_2O and deuterium in D_2O $\nu(D)/\nu(p) = 0.153\,506\,083(60)$ [27], the diamagnetic shielding constant for Sc^{3+} in $ScCl_3 \sigma(^{45}\text{Sc}) = 0.001\,56(10)$ [28] and proton in water $\sigma(p) = 25.687(15) \times 10^{-6}$ [29], and magnetic moment of proton $\mu(p) = +2.792\,847\,337(29)\mu_N$

TABLE II. Ground-state electromagnetic moments of ^{40,41,45}Sc. The ^{41}Sc electromagnetic moments were deduced from the weighted average of the moments calculated using the upper- and lower-level hyperfine coupling constants of both the $^3D_2 \leftrightarrow {}^3F^\circ_3$ and $^3D_1 \leftrightarrow {}^3P_0$ transitions. Previously measured values of the ^{41,45}Sc electromagnetic moments are also included in the table. The signs are not assigned experimentally, where it is given in parentheses.

		μ (μ_N)		Q (e^2fm^2)	
Isotope	I^π	This work	Lit.	This work	Lit.
^{40}Sc	4^-	+5.57(4)(2)		+42(38)(28)	
^{41}Sc	$7/2^-$	+5.4376(80)(06)	(+)5.431(2) [11]	−18.5(71)(01)	(−)15.6(3) [23]
^{45}Sc	$7/2^-$		+4.7563(5)[a]		−23.6(2)[b]

[a]This value was re-evaluated based on Ref. [24] in the present work. See text for detail.
[b]This value was re-evaluated in Ref. [23].

[29], the magnetic moment of ^{45}Sc can be obtained [30] as

$$\mu(^{45}\mathrm{Sc}) = \frac{\nu(^{45}\mathrm{Sc})}{\nu(p)}\frac{1-\sigma(p)}{1-\sigma(^{45}\mathrm{Sc})}\frac{I(^{45}\mathrm{Sc})}{I(p)}\mu(p) = +4.75631(48)\mu_N.$$

Together with our present measurement of $A^{\mathrm{hf}}(^{45}\mathrm{Sc}) = +507.54(2)(4)$ MHz, the ground-state magnetic moment of ^{40}Sc ($I^\pi = 4^-$) was deduced from Eq. (10) to be

$$\mu(^{40}\mathrm{Sc}) = +5.57(4)(2)\mu_N,$$

which is also summarized in Table II. Here the correlation between the variation of A^{hf} due to possible variation of B^{hf} was taken into account and propagated in the systematic uncertainty of the present $\mu(^{40}\mathrm{Sc})$.

D. Electric-quadrupole moment

The electric-quadrupole hyperfine coupling constant of ^{40}Sc was obtained as

$$B^{\mathrm{hf}}(^3\mathrm{D}_2) = +58(52)(39)\ \mathrm{MHz}.$$

The quadrupole moment of ^{40}Sc can be deduced from Eq. (8) together with the present $B^{\mathrm{hf}}(^3\mathrm{D}_2)$ for ^{40}Sc and ^{45}Sc, and the quadrupole moment of ^{45}Sc as

$$Q(^{40}\mathrm{Sc}) = Q(^{45}\mathrm{Sc})\frac{B^{\mathrm{hf}}(^{40}\mathrm{Sc})}{B^{\mathrm{hf}}(^{45}\mathrm{Sc})}. \tag{11}$$

Using values of our measurement of $B^{\mathrm{hf}}(^{45}\mathrm{Sc}) = -32.63(21)(15)$ MHz, $Q(^{45}\mathrm{Sc}) = -23.6(2)\ e\,\mathrm{fm}^2$ [23], the ground-state quadrupole moment of ^{40}Sc ($I^\pi = 4^-$) was deduced to be

$$Q(^{40}\mathrm{Sc}) = +42(38)(28)\ e\,\mathrm{fm}^2.$$

No further meaningful discussion can be made for the quadrupole moment of ^{40}Sc due to the large uncertainty. All values are summarized in Table II.

V. DISCUSSION

A. Shell-model calculations

The magnetic moment operator can be expressed as

$$\boldsymbol{\mu} = g_s\boldsymbol{s} + g_l\boldsymbol{l}, \tag{12}$$

where g_s and g_l are the spin and the orbital g factors, respectively. The free nucleon g factors ($g_l^{\mathrm{p}} = 1$, $g_l^{\mathrm{n}} = 0$, $g_s^{\mathrm{p}} = 5.586$, and $g_s^{\mathrm{n}} = -3.826$) were used for the calculation. For the magnetic moment of ^{40}Sc we used a shell-model space for one proton in the full fp shell ($0f_{7/2}, 0f_{5/2}, 1p_{3/2}, 1p_{1/2}$), and one neutron hole in the full sd shell ($0d_{3/2}, 1s_{1/2}, 0d_{5/2}$) with the $sdpf$-wb effective shell-model interactions [34]. The $I^\pi = 4^-$ ground-state magnetic moment with the full wave function was obtained as

$$\mu(^{40}\mathrm{Sc})_{\mathrm{full}} = 5.936\ \mu_N.$$

This model space and interaction were also used recently with regard to high-spin states in ^{40}Sc [35]. The 4^- wave function of the ground state is dominated (97.97%) by the canonical $(\pi : 0f_{7/2})(\nu : 0d^{-1}_{3/2})$ configuration. For this almost pure configuration we can use the additivity rule to obtain the magnetic moments of ^{40}Sc. According to Eq. (3) we obtain

$$\mu(^{40}\mathrm{Sc}) = \frac{32}{35}\ \mu_p(0f_{7/2}) + \frac{8}{15}\ \mu_n\big(0d^{-1}_{3/2}\big).$$

Using the single-particle magnetic moments of $\mu_p(0f_{7/2})$ and $\mu_n(0d^{-1}_{3/2})$ obtained from Eq. (1), this pure configuration has a free-nucleon single-particle (sp) magnetic moment (in units of μ_N) of

$$\mu(^{40}\mathrm{Sc})_{\mathrm{sp}} = \frac{32}{35}\ 5.793 + \frac{8}{15}\ 1.148 = 5.909.$$

Alternatively we can evaluate to some approximation the pure configuration using known experimental ground-state magnetic moments of ^{41}Sc($7/2^-$) [11] and ^{39}Ca($3/2^+$) [32] for the $\mu_p(0f_{7/2})$ and $\mu_n(0d^{-1}_{3/2})$, respectively. This would take into account the components for the wave function that go beyond one-particle one-hole configuration, and mesonic exchange corrections to the free nucleon g factors. In a unit of μ_N this magnetic moment (pure) is given

$$\mu(^{40}\mathrm{Sc})_{\mathrm{pure}} = \frac{32}{35}\ 5.431(2) + \frac{8}{15}\ 1.0217(1) = 5.510(2),$$

where numbers in the parentheses are experimental uncertainties of magnetic moments, which are small compared with the present result and will be ignored hereafter.

The difference of the calculated magnetic moment of the full particle-hole configuration and the simple single-particle $(0f_{7/2})(0d^{-1}_{3/2})$ configuration with free nucleon g factors is $\mu_{\mathrm{full}} - \mu_{\mathrm{sp}} = 0.028\mu_N$. Adding this small difference

TABLE III. Shell-model and multishell in-medium similarity renormalization group calculations for magnetic moment of the 4^- ground state in ^{40}Sc and ^{40}K, together with their experimental values (Expt.). Magnetic moments of the $A = 39$ and 41 systems are also listed to obtain values based on the additivity rule. All values are given in units of μ_N. For the shell model, sp, full and emp are for the single-particle, full, and corrected empirical calculations, respectively. For the Expt., values under pure are obtained using additivity rule with experimental values. See text for more details.

	Shell model			IMSRG				
	sp	full	emp	EM[a]	NNLO[b]	N3LO[c]	Expt.	Ref.
$\mu(^{40}\mathrm{K})$		-1.707[d]		-1.337	-1.096	-1.327	$-1.2981(0)$	[31]
$\mu(^{40}\mathrm{Sc})$		5.936[e]		5.585	5.400	5.583	$+5.57(4)(2)$	Present
μ_{IS}		2.115		2.124	2.152	2.128	$+2.136(20)$	
$\langle s_3\rangle$		0.301		0.326	0.399	0.337	$+0.358(53)$	
μ_{IV}		3.822		3.461	3.248	3.455	$+3.434(20)$	
$\mu(^{39}\mathrm{K})$	0.124	-0.469		-0.019	0.025	-0.034	$-0.3915(0)$	[31]
$\mu(^{39}\mathrm{Ca})$	1.148	0.930		1.337	1.326	1.369	$(+)1.0217(1)$	[32]
$\mu(^{41}\mathrm{Ca})$	-1.913	-2.021		-1.308	-1.236	-1.320	$-1.5947(0)$	[33]
$\mu(^{41}\mathrm{Sc})$	5.793	5.813		5.199	5.113	5.203	$(+)5.431(2)$	[11]
			Using additivity rule				pure	
$\mu(^{40}\mathrm{K})$	-1.683	-1.598	-1.273	-1.206	-1.116	-1.224	$-1.2492(0)$	
$\mu(^{40}\mathrm{Sc})$	5.909	5.811	5.538	5.476	5.382	5.487	$(+)5.510(2)$	
μ_{IS}	2.113	2.11	2.133	2.130	2.133	2.131	$(+)2.131(1)$	
$\langle s_3\rangle$	0.297	0.28	0.349	0.342	0.350	0.345	$(+)0.344(2)$	
μ_{IV}	3.796	3.70	3.406	3.336	3.249	3.356	$(+)3.380(1)$	

[a]1.8/2.0(EM).
[b]NNLOgo(394).
[c]N3LO$_{lnl}$.
[d]Calculated with free nucleon g factors.
[e]Calculated with free nucleon g factors.

to $\mu(^{40}\mathrm{Sc})_{\mathrm{pure}}$, we obtain a corrected magnetic moment as

$$\mu(^{40}\mathrm{Sc})_{\mathrm{emp}} = 5.538\mu_N.$$

This is an empirical shell-model (emp) value obtained within the additivity rule corrected for the configuration mixing and meson-exchange effect, which is in good agreement with the present experimental value of $5.57(4)(2)\mu_N$. The results are summarized in Table III and Fig. 2 together with results of similar analysis for the mass $A = 40$ mirror nucleus $^{40}\mathrm{K}(4^-)$, whose ground-state magnetic moment is known [31]. Here magnetic moments of $^{39}\mathrm{K}(3/2^+)$ [31] and $^{41}\mathrm{Ca}(7/2^-)$ [33] were used as the pure configuration for the $\mu_p(0d_{3/2}^{-1})$ and $\mu_n(0f_{7/2})$, respectively, to extract the $\mu(^{40}\mathrm{K})_{\mathrm{emp}}$ from the additivity rule. The magnetic moment calculated using the additivity rule with the correction $\mu_{\mathrm{full}} - \mu_{\mathrm{sp}} = -0.024\mu_N$ agrees well with the experimental value. For both magnetic moments of ^{40}Sc and ^{40}K, the μ_{sp} and μ_{full} deviate significantly from the experimental value, indicating departure from the canonical configuration and needs for mesonic effects. Note that calculations for ^{40}K show larger deviation from the experimental magnetic moment than those for ^{40}Sc.

The magnetic moments for the $A = 39$ obtained with the empirical *sd* shell effective g factors [36] and for the $A = 41$ obtained with the empirical fp shell effective g factors [37] are also summarized in Table III as “full.” The magnetic moments for $A = 40$ deduced using these values using the additivity rule are also listed in Table III and shown in Fig. 2 as “full add.” The magnetic moments obtained with the effective g factors are slightly closer to the experimental values than those with the free g factors (sp) and the full calculations, but still deviates significantly from the experimental values. These differences from experiment may be due to excitations of nucleons from *sd* to fp shell in nuclei near ^{40}Ca [11,12] that are in excess of those present in the middle of the *sd* and fp shells. Our analysis shows that these excess excitations do not change the additivity relationships expected from the simple particle-hole wave functions as can be seen from the good agreement of the empirical shell-model calculations with the experimental value of magnetic moments.

B. *Ab initio* in-medium similarity renormalization group calculation

In addition, we provide ab initio magnetic moments from the valence-space formulation of the *ab initio* in-medium similarity renormalization group (VS-IMSRG) [38,39] based on input two- and three-nucleon forces from chiral effective field theory (EFT) [40,41]. *Ab initio* calculations of electromagnetic properties have progressed to regions near the *sd* shell [12,42–45], where notable, but largely understood, discrepancies have emerged compared with data. Using the Magnus approach [46], we generate an approximate unitary transformation to decouple a given core and valence-space Hamiltonian from the full-space Hamiltonian, where operators are truncated at the two-body level [IMSRG(2)], and

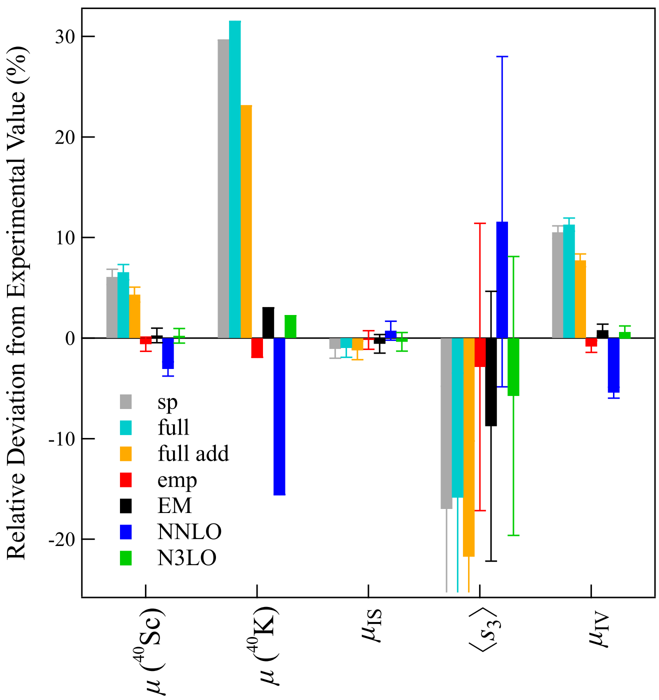

FIG. 2. Relative deviations of theoretical magnetic moments from experimental values are shown. The sp, full, emp are for the single particle, full, and empirical shell-model calculations, respectively (see text for more detail). The EM, NNLO, and N3LO are for In-medium similarity renormalization group (IMSRG) calculations with 1.8/2.0(EM), NNLOgo(394) and N3LO$_{lnl}$ interactions, respectively. Uncertainties are also included, which are dominated by the experimental uncertainty in the present $\mu(^{40}Sc)$.

$3N$ forces between valence nucleons is captured via ensemble normal ordering [47]. The same transformation is used to decouple effective valence-space $M1$ operators consistent with the Hamiltonian [48], in principle eliminating the need for quenching typically seen in phenomenological approaches. We note, however, that effects of two-body currents are expected to be non-negligible but are not currently implemented.

We start from a harmonic-oscillator basis of 15 major shells and use three different $NN + 3N$ interactions derived from chiral EFT. First the 1.8/2.0(EM) [49,50] and N3LO$_{lnl}$ are known to well reproduce ground-state energies globally to the tin region [51,52], while underpredicting charge radii [53]. The NNLOgo(394) interaction includes explicit delta isobar degrees of freedom [54] and generally exhibits improved radii properties without sacrificing energies [55,56]. Since the physics of ^{40}Sc is expected to span the *sd* and *pf* shells, we use the newly formulated multishell approach [57] to decouple a valence-space Hamiltonian and effective $M1$ operator above a ^{28}Si core, in an increased $E_{3\max} = 24$ truncation on storage of $3N$ matrix elements [58]. Finally, energies and moments are obtained from the *K*SHELL shell-model code [59], where only free g factors are used. Although effects of two-body current are not included in the calculations, the overall agreement with experimental magnetic moments of ^{40}K and ^{40}Sc are good, but the NNLOgo(394) interaction, which shows larger deviation from experimental value than other two interactions, especially for ^{40}K.

C. Isoscalar and isovector magnetic moments

Examination of only the contribution from the isoscalar (IS) and isovector (IV) parts of the magnetic moment can also provide insight into shell structure and configuration mixing. The IS and IV magnetic moment can be obtained from mirror magnetic moments as

$$\mu_{IS} = \tfrac{1}{2}\{\mu(T_3 = +T) + \mu(T_3 = -T)\},$$
$$\mu_{IV} = \tfrac{1}{2}\{\mu(T_3 = +T) - \mu(T_3 = -T)\}, \tag{13}$$

with the isospin $T_3 = +1/2$ for protons. Assuming good isospin symmetry and ignoring the isoscalar mesonic exchange currents, the isoscalar spin expectation value $\langle s_3\rangle$ [60,61], which is the contribution of nuclear spins to the magnetic moment, can also be evaluated from the μ_{IS} as $\langle s_3\rangle = (\mu_{IS} - I/2)/(g_p^s + g_n^s - g_p^l)$, where g_p^s, g_n^s, and g_p^l are the free proton and neutron g factors, respectively, and $\langle\,\rangle$ indicates a sum over all nucleons. The μ_{IS}, μ_{IV}, and $\langle s_3\rangle$ each extracts a specific part of the magnetic moment operator and amplifies small differences in experimental and theoretical values, and therefore are more sensitive to small changes in the magnetic moments of the mirror pair. The present $\mu(^{40}Sc)$ was combined with the existing magnetic moment of $\mu(^{40}K)$ [31], and μ_{IS}, μ_{IV}, and $\langle s_3\rangle$ were obtained, which are summarized in Table III and Fig. 2 together with the shell-model and IMSRG calculations.

Good agreements were achieved for μ_{IS} and μ_{IV} between experiment and shell-model calculations with the empirical shell-model values evaluated using the additivity rule. $\langle\sigma_3\rangle$ has large uncertainty due to the uncertainty in the present $\mu(^{40}Sc)$, and no further discussion is given here. The IMSRG calculations show similarly good agreement except for the NNLOgo(394) interaction. It can be seen that μ_{IS} is insensitive to the different set of calculations, including the single-particle value, and shows only slight variation within the experimental uncertainties. On the other hand, calculated values of μ_{IV} deviate more and dominate the discrepancy of the magnetic moment from the experimental value.

VI. SUMMARY

Bunched-beam collinear laser spectroscopy was performed to determine electromagnetic moments of the 4^- ground state in the odd-odd ^{40}Sc nucleus, occurring at the proton drip line. The hyperfine structure of the $^3D_2 \leftrightarrow {}^3F_3^\circ$ transition in the singly charged ^{40}Sc was measured, and the magnetic-dipole and electric-quadrupole hyperfine coupling constants were deduced. Magnetic moments obtained by the additivity rule using empirical magnetic moments of neighboring odd-even nuclei and shell-model corrections well reproduce the experimental magnetic moment of ^{40}Sc, and the mirror nucleus ^{40}K. The *ab initio* multishell IMSRG calculations were also performed for the magnetic moments, which show good agreement with experimental values except the NNLOgo(394) interaction. However, the good agreement should be further confirmed with the inclusion of mesonic contributions, which are not included in the present calculations. The isoscalar and isovector magnetic moments were deduced with the known magnetic moment of mirror ^{40}K nucleus. $\mu_{\rm IS}$ is insensitive to the calculations employed in the present study, but $\mu_{\rm IV}$ deviates more and dominates the departure from experimental magnetic moments. Note that the shell-model calculations for the $A = 39$ and 41 doubly magic plus or minus one nucleon nuclei deviate from their experimental values, which indicates missing nucleon excitation across the *sd* and *fp* major shells. The good agreement of the empirical shell-model calculations with the present ^{40}Sc magnetic moment and the analysis of the additivity rule can be regarded that the additivity rule is still applicable for such systems, where cross shell excitation has considerable contribution to magnetic moments. The electric-quadrupole moment of ^{40}Sc was deduced from the present hyperfine coupling constant, but no further discussion was given due to large statistical uncertainty.

ACKNOWLEDGMENTS

This work was supported in part by the National Science Foundation, Grants No. PHY-15-65546, No. PHY-19-13509, No. PHY-21-10365 and No. PHY-21-11185; Natural Sciences and Engineering Research Council of Canada Grants SAPIN-2018-00027 and RGPAS-2018-522453; the Deutsche Forschungsgemeinschaft (DFG, German Research Foundation) – Project-ID 279384907 – SFB 1245. TRIUMF receives funding via a contribution through the National Research Council of Canada. J.D.H. and T.M. would like to thank S. R. Stroberg for the imsrg++ code used to perform VS-IMSRG calculations. The VS-IMSRG calculations were performed with an allocation of computing resources on Cedar at WestGrid and Compute Canada and on the Oak Cluster at TRIUMF managed by the University of British Columbia, Department of Advanced Research Computing.

[1] Von Th. Schmidt, Über die magnetischen momente der Atomkerne, Z. Physik **106**, 358 (1937).

[2] C. Woods, W. Catford, L. Fifield, and N. Orr, A measurement of the mass of ^{39}Sc, Nucl. Phys. A **484**, 145 (1988).

[3] K. Sugimoto, Nuclear moments of conjugate nuclei, J. Phys. Soc. Jpn. Suppl. **34**, 197 (1973).

[4] K. Matsuta, T. Minamisono, M. Tanigaki, M. Fukuda, Y. Nojiri, M. Mihara, T. Onishi, T. Yamaguchi, A. Harada, M. Sasaki, T. Miyake, K. Minamisono, T. Fukao, K. Sato, Y. Matsumoto, T. Ohtsubo, S. Fukuda, S. Momota, K. Yoshida, A. Ozawa *et al.*, Magnetic moments of proton drip-line nuclei ^{13}O and ^{9}C, Hyperfine Interact. **97/98**, 519 (1996).

[5] M. Huhta, P. F. Mantica, D. W. Anthony, B. A. Brown, B. S. Davids, R. W. Ibbotson, D. J. Morrissey, C. F. Powell, and M. Steiner, Anomalous *p*-shell isoscalar magnetic moments: Remeasurement of ^{9}C and the influence of isospin nonconservation, Phys. Rev. C **57**, R2790(R) (1998).

[6] Y. Utsuno, Anomalous magnetic moment of ^{9}C and shell quenching in exotic nuclei, Phys. Rev. C **70**, 011303(R) (2004).

[7] E. Feenberg, Notes on the $j - j$ coupling shell model, Phys. Rev. **76**, 1275 (1949).

[8] P. F. A. Klinkenberg, Tables of nuclear shell structure, Rev. Mod. Phys. **24**, 63 (1952).

[9] N. Stone, Table of nuclear magnetic dipole and electric quadrupole moments, At. Data Nucl. Data Tables **90**, 75 (2005).

[10] O. I. Achakovskiy, S. P. Kamerdzhiev, E. E. Saperstein, and S. V. Tolokonnikov, Magnetic moments of odd-odd spherical nuclei, Eur. Phys. J. A **50**, 6 (2014).

[11] T. Minamisono, Y. Nojiri, K. Matsuta, K. Takeyama, A. Kitagawa, T. Ohtsubo, A. Ozawa, and M. Izumi, Precision measurement of the magnetic moment of ^{41}Sc($I^\pi = 7/2^-$, $T_{1/2} =$ 0.59 s) and isoscalar *g* factors of orbital and spin angular momenta, Nucl. Phys. A **516**, 365 (1990).

[12] A. Klose, K. Minamisono, A. J. Miller, B. A. Brown, D. Garand, J. D. Holt, J. D. Lantis, Y. Liu, B. Maaß, W. Nörtershäuser, S. V. Pineda, D. M. Rossi, A. Schwenk, F. Sommer, C. Sumithrarachchi, A. Teigelhöfer, and J. Watkins, Ground-state electromagnetic moments of ^{37}Ca, Phys. Rev. C **99**, 061301(R) (2019).

[13] A. Bohr and V. F. Weisskopf, The influence of nuclear structure on the hyperfine structure of heavy elements, Phys. Rev. **77**, 94 (1950).

[14] D. J. Morrissey, B. M. Sherrill, M. Steiner, A. Stolz, and I. Wiedenhoever, Commissioning the A1900 projectile fragment separator, Nucl. Instrum. Methods Phys. Res., Sect. B **204**, 90 (2003).

[15] C. S. Sumithrarachchi, D. J. Morrissey, S. Schwarz, K. Lund, G. Bollen, R. Ringle, and G. Savard, Beam thermalization in a large gas catcher, Nucl. Instrum. Methods Phys. Res., Sect. B **463**, 305 (2020).

[16] K. Minamisono, P. F. Mantica, A. Klose, S. Vinnikova, A. Schneider, B. Johnson, and B. R. Barquest, Commissioning of the collinear laser spectroscopy system in the BECOLA facility at NSCL, Nucl. Instrum. Methods Phys. Res., Sect. A **709**, 85 (2013).

[17] D. M. Rossi, K. Minamisono, B. R. Barquest, G. Bollen, K. Cooper, M. Davis, K. Hammerton, M. Hughes, P. F. Mantica, D. J. Morrissey, R. Ringle, J. A. Rodriguez, C. A. Ryder, S. Schwarz, R. Strum, C. Sumithrarachchi, D. Tarazona, and S. Zhao, A field programmable gate array-based time-resolved scaler for collinear laser spectroscopy with bunched radioactive potassium beams, Rev. Sci. Instrum. **85**, 093503 (2014).

[18] B. R. Barquest, G. Bollen, P. F. Mantica, K. Minamisono, R. Ringle, and S. Schwarz, RFQ beam cooler and buncher for collinear laser spectroscopy of rare isotopes, Nucl. Instrum. Method Phys. Res. A **866**, 18 (2017).

[19] P. Campbell, H. L. Thayer, J. Billowes, P. Dendooven, K. T. Flanagan, D. H. Forest, J. A. R. Griffith, J. Huikari, A. Jokinen, R. Moore, A. Nieminen, G. Tungate, S. Zemlyanoi, and J. Äystö, Laser Spectroscopy of Cooled Zirconium Fission Fragments, Phys. Rev. Lett. **89**, 082501 (2002).

[20] A. Nieminen, P. Campbell, J. Billowes, D. H. Forest, J. A. R. Griffith, J. Huikari, A. Jokinen, I. D. Moore, R. Moore, G. Tungate, and J. Äystö, On-Line Ion Cooling and Bunching for Collinear Laser Spectroscopy, Phys. Rev. Lett. **88**, 094801 (2002).

[21] B. Maaß, K. König, J. Krämer, A. J. Miller, K. Minamisono, W. Nörtershäuser, and F. Sommer, A 4π fluorescence detection region for collinear laser spectroscopy, arXiv:2007.02658.

[22] C. A. Ryder, K. Minamisono, H. B. Asberry, B. Isherwood, P. F. Mantica, A. Miller, D. M. Rossi, and R. Strum, Population distribution subsequent to charge exchange of 29.85 keV Ni^+ on sodium vapor, Spectrochim. Acta, Part B **113**, 16 (2015).

[23] T. Minamisono *et al.*, Quadrupole moments of the ^{40}Ca core plus one nucleon nuclei ^{41}Sc and ^{41}Ca, Z. Naturforsch. A **57**, 595 (2002).

[24] O. Lutz, The magnetic moment of ^{45}scandium, Phys. Lett. A **29**, 58 (1969).

[25] K. König, K. Minamisono, J. Lantis, S. Pineda, and R. Powel, Beam energy determination via collinear laser spectroscopy, Phys. Rev. A **103**, 032806 (2021).

[26] J. R. Persson, Table of hyperfine anomaly in atomic systems, At. Data Nucl. Data Tables **99**, 62 (2013).

[27] B. Smaller, Precise determination of the magnetic moment of the deuteron, Phys. Rev. **83**, 812 (1951).

[28] W. R. Johnson, D. Kolb, and K.-N. Huang, Electric- dipole, quadrupole, and magnetic-dipole susceptibilities and shielding factors for closed-shell ions of the He Ne, Ar, Ni(Cu^+), Kr, Pb, and Xe isoelectronic sequences, At. Data Nucl. Data Tables **28**, 333 (1983).

[29] P. J. Mohr, D. B. Newell, and B. N. Taylor, CODATA recommended values of the fundamental physical constants 2014, Rev. Mod. Phys. **88**, 035009 (2016).

[30] A. Antušek *et al.*, Nuclear magnetic dipole moments from NMR spectra, Chem. Phys. Lett. **411**, 111 (2005).

[31] W. Sahm and A. Schwenk, ^{39}K, ^{40}K and ^{41}K nuclear magnetic resonance studies, Z. Naturforsch. A **29**, 1754 (1974).

[32] T. Minamisono, J. W. Hugg, D. G. Mavis, T. K. Saylor, H. F. Glavish, and S. S. Hanna, Measurement of the magnetic moment of ^{39}Ca by use of a polarized proton beam and NMR detection, Phys. Lett. B **61**, 155 (1976).

[33] E. Brun, J. J. Kraushaar, W. L. Pierce, and W. J. Veigele, Nuclear Magnetic Dipole Moment of Ca^{41} Phys. Rev. Lett. **9**, 166 (1962).

[34] E. K. Warburton, J. A. Becker, and B. A. Brown, Mass systematics for $A = 29$–44 nuclei: The deformed $A \approx 32$ region, Phys. Rev. C **41**, 1147 (1990).

[35] A. Gade, D. Weisshaar, B. Brown, J. Tostevin, D. Bazin, K. Brown, R. Charity, P. Farris, A. Hill, J. Li, B. Longfellow, W. Reviol, and D. Rhodes, In-beam γ-ray spectroscopy at the proton dripline: ^{40}Sc, Phys. Lett. B **808**, 135637 (2020).

[36] W. A. Richter, S. Mkhize, and B. A. Brown, sd-shell observables for the USDA and USDB Hamiltonians, Phys. Rev. C **78**, 064302 (2008).

[37] M. Honma, T. Otsuka, B. A. Brown, and T. Mizusaki, New effective interaction for pf-shell nuclei and its implications for the stability of the $N = Z = 28$ closed core, Phys. Rev. C **69**, 034335 (2004).

[38] H. Hergert, S. K. Bogner, T. D. Morris, A. Schwenk, and K. Tsukiyama, The in-medium similarity renormalization group: A novel *ab initio* method for nuclei, Phys. Rep. **621**, 165 (2016).

[39] S. R. Stroberg, S. K. Bogner, H. Hergert, and J. D. Holt, Non-empirical interactions for the nuclear shell model: An update, Annu. Rev. Nucl. Part. Sci. **69**, 307 (2019).

[40] E. Epelbaum, H.-W. Hammer, and Ulf-G. Meißner, Modern theory of nuclear forces, Rev. Mod. Phys. **81**, 1773 (2009).

[41] R. Machleidt and D. R. Entem, Chiral effective field theory and nuclear forces, Phys. Rep. **503**, 1 (2011).

[42] J. Henderson *et al.*, Testing microscopically derived descriptions of nuclear collectivity: Coulomb excitation of ^{22}Mg, Phys. Lett. B **782**, 468 (2018).

[43] S. Heil, M. Petri, K. Vobig *et al.*, Electromagnetic properties of ^{21}O for benchmarking nuclear Hamiltonians, Phys. Lett. B **809**, 135678 (2020).

[44] M. Ciemala, S. Ziliani, F. C. L. Crespi *et al.*, Testing *ab initio* nuclear structure in neutron-rich nuclei: Lifetime measurements of second 2^+ states in ^{16}C and ^{20}O, Phys. Rev. C **101**, 021303 (2020).

[45] H. Heylen, C. S. Devlin, W. Gins, M. L. Bissell, K. Blaum, B. Cheal, L. Filippin, R. F. Ruiz, M. Godefroid, C. Gorges, J. D. Holt, A. Kanellakopoulos, S. Kaufmann, Á. Koszorús, K. König, S. Malbrunot-Ettenauer, T. Miyagi, R. Neugart, G. Neyens, W. Nörtershäuser, R. Sánchez, F. Sommer, L. V. Rodríguez, L. Xie, Z. Y. Xu, X. F. Yang, and D. T. Yordanov, High-resolution laser spectroscopy of $^{27-32}$Al, Phys. Rev. C **103**, 014318 (2021).

[46] T. D. Morris, N. M. Parzuchowski, and S. K. Bogner, Magnus expansion and in-medium similarity renormalization group, Phys. Rev. C **92**, 034331 (2015).

[47] S. R. Stroberg, A. Calci, H. Hergert, J. D. Holt, S. K. Bogner, R. Roth, and A. Schwenk, Nucleus-Dependent Valence-Space Approach to Nuclear Structure, Phys. Rev. Lett. **118**, 032502 (2017).

[48] N. M. Parzuchowski, S. R. Stroberg, P. Navratil, H. Hergert, and S. K. Bogner, *Ab initio* electromagnetic observables with the in-medium similarity renormalization group, Phys. Rev. C **96**, 034324 (2017).

[49] K. Hebeler, S. K. Bogner, R. J. Furnstahl, A. Nogga, and A. Schwenk, Improved nuclear matter calculations from chiral low-momentum interactions, Phys. Rev. C **83**, 031301(R) (2011).

[50] J. Simonis, S. R. Stroberg, K. Hebeler, J. D. Holt, and A. Schwenk, Saturation with chiral interactions and consequences for finite nuclei, Phys. Rev. C **96**, 014303 (2017).

[51] T. D. Morris, J. Simonis, S. R. Stroberg, C. Stumpf, G. Hagen, J. D. Holt, G. R. Jansen, T. Papenbrock, R. Roth, and A. Schwenk, Structure of the Lightest Tin Isotopes, Phys. Rev. Lett. **120**, 152503 (2018).

[52] S. R. Stroberg, J. D. Holt, A. Schwenk, and J. Simonis, *Ab Initio* Limits of Atomic Nuclei, Phys. Rev. Lett. **126**, 022501 (2021).

[53] R. de Groote *et al.*, Measurement and microscopic description of odd-even staggering of charge radii of exotic copper isotopes, Nat. Phys. **16**, 620 (2020).

[54] W. G. Jiang, A. Ekstrom, C. Forssen, G. Hagen, G. R. Jansen, and T. Papenbrock, Accurate bulk properties of nuclei from $a = 2$ to ∞ from potentials with Δ isobars, Phys. Rev. C **102**, 054301 (2020).

[55] A. Koszorús, X. F. Yang, W. G. Jiang *et al.*, Charge radii of exotic potassium isotopes challenge nuclear theory and the magic character of $N = 32$, Nat. Phys. **17**, 439 (2021).

[56] M. Mougeot *et al.*, Mass measurements of $^{99-101}$In challenge *ab initio* nuclear theory of the nuclide ^{100}Sn, Nat. Phys. **17**, 1099 (2021).

[57] T. Miyagi, S. R. Stroberg, J. D. Holt, and N. Shimizu, *Ab initio* multishell valence-space Hamiltonians and the island of inversion, Phys. Rev. C **102**, 034320 (2020).
[58] T. Miyagi, S. R. Stroberg, P. Navrátil, K. Hebeler, and J. D. Holt, *Ab initio* limits of atomic nuclei, Phys. Rev. C **105**, 014302 (2022).
[59] N. Shimizu, T. Mizusaki, Y. Utsuno, and Y. Tsunoda, Thick-restart block Lanczos method for large-scale shell-model calculations, Comput. Phys. Commun. **244**, 372 (2019).
[60] R. G. Sachs, The magnetic moments of light nuclei, Phys. Rev. **69**, 611 (1946).
[61] K. Sugimoto, Magnetic moments and β-decay ft values of mirror nuclei, Phys. Rev. **182**, 1051 (1969).